

Low-Threshold Amplified Spontaneous Emission and Lasing from Thick-Shell CdSe/CdS Core/Shell Nanoplatelets Enabled by High-Temperature Growth

Lei Zhang, Hongyu Yang, Buyang Yu, Ying Tang, Chunfeng Zhang,* Xiaoyong Wang,* Min Xiao, Yiping Cui, and Jiayu Zhang*

Colloidal semiconductor nanoplatelets (NPLs) have recently emerged as highly promising optical gain medium because of their superior optical properties. Here, the shell-thickness-dependent optical gain properties of CdSe/CdS core/shell NPLs synthesized by high-temperature growth are systematically investigated for the first time. The core/shell NPLs show the increased quantum yields and enhanced photostability as well as clear reduced emission blinking, thanks to the preferable passivation of nonradiative surface defects by the growth of the high-quality CdS shells under high reaction temperature. Meanwhile, the amplified spontaneous emission (ASE) performance of CdSe/CdS NPLs indicates a nonmonotonic dependence on the shell thickness. The ASE threshold is achieved as low as $\approx 4.4 \mu\text{J cm}^{-2}$ for thick-shell NPLs with six monolayer CdS shells, and exhibiting ultrafast transient dynamics process (≈ 11 ps). Besides, an extremely long lifetime (>800 ps) and large bandwidth (>140 nm) of optical gain are observed by employing ultrafast transient absorption spectroscopy. Finally, a thick-shell NPLs vertical cavity surface-emitting laser is developed, which demonstrates spatially directional single-mode operation with an ultralow lasing threshold of $\approx 1.1 \mu\text{J cm}^{-2}$. These excellent results are attributed to the remarkable optical gain performance of core/shell NPLs and represent an important step toward practical NPL laser devices.

quantum wells, because of their precisely nanometer-scale thickness just with a few atomic monolayers (MLs).^[1–3] The excitons in NPLs are free to move within the plane and just confined in thickness dimensions, which exhibits strong 1D quantum confinement effect.^[3,4] Thus, the NPLs have the characteristic photophysical properties, including the fast radiative decay rates, narrower photoluminescence (PL) emission spectra, larger absorption cross sections, and giant oscillator strengths.^[3,5–8] All these superior properties are highly desired for their promising light-emitting diodes^[9–11] and lasing applications.^[12–15]

The properties of colloidal core-only NPL materials could be further improved in core/shell or core/crow heterostructures.^[13,15–20] Among these, CdSe/CdS core/shell NPLs have been increasingly attractive due to their excellent shell-thickness-dependent optical performance.^[13,17,20–22] CdSe/CdS NPLs are synthesized with higher quantum yields (QYs) and stability as compared to CdSe core-only NPLs, because of the effective passivation

of surface trap states by the epitaxial growth of a wider bandgap shells.^[17,23,24] In addition to the passivated surface defects, the absorption cross section of CdSe/CdS NPLs was boosted owing to the intrinsically increased optical absorption of the CdS shells.^[20] At the same time, the inorganic shells could help to suppress the rapid nonradiative Auger recombination (AR) of excitons with lower Auger rates and much reduced emission intermittency at single particle level, thereby enabling to realize low-threshold ($\approx 6 \mu\text{J cm}^{-2}$) amplified spontaneous emission (ASE) and obtain high threshold for gain saturation.^[13,16,20,22,23,25] Generally, the epitaxial growth of semiconductor shells in core/shell hetero-nanoplatelets is performed via the colloidal atomic layer deposition (c-ALD) method.^[26–29] However, as c-ALD usually takes place at room temperature, such synthetic approach allows for CdSe/CdS NPLs with only limited QYs (≈ 20 – 40%) and stability.^[26,29,30] These properties need to be improving for ensuring their applications in colloidal optoelectronic devices.


Fortunately, several routes of synthesizing CdSe-based core/shell heterostructure NPLs have proved that the hot-injection

1. Introduction

Colloidal semiconductor 2D nanoplatelets (NPLs) is a kind of novel nanomaterials similar to the electronic structure of

L. Zhang, H. Yang, Prof. Y. Cui, Prof. J. Zhang
Advanced Photonics Center
Southeast University
Nanjing 210096, China
E-mail: jy Zhang@seu.edu.cn

B. Yu, Y. Tang, Prof. C. Zhang, Prof. X. Wang, Prof. M. Xiao
National Laboratory of Solid State Microstructures
School of Physics, and Collaborative Innovation Center of Advanced Microstructures
Nanjing University
Nanjing 210093, China
E-mail: cf Zhang@nju.edu.cn; wxiaoyong@nju.edu.cn

 The ORCID identification number(s) for the author(s) of this article can be found under <https://doi.org/10.1002/adom.201901615>.

DOI: 10.1002/adom.201901615

shell growth scheme could enormously improve the optical properties of core/shell NPLs in comparison with that under low reaction temperatures.^[30,31] The experiments show that the high-temperature synthesis of CdSe/CdS core/shell NPLs is conducive to allow the growth of highly uniform and thick inorganic shells. Importantly, the highly crystalline shells from the slow deposition process at high temperature would reduce the surface nonradiative recombination by better passivating surface traps, which could also result in minimal interfacial defects by atomic diffusion and reorganization at the same time.^[30–32] Thus, in contrast to conventional c-ALD method, the high-temperature shell growth approach could result in CdSe-based core/shell NPLs with narrow emission bandwidth, improved QYs ($\approx 60\%$ for CdSe/CdS NPLs and $\approx 98\%$ for CdSe/ZnS NPLs) and enhanced optical stability, as well as exhibiting preminent ASE performance after being annealed at 500 K.^[30,31] The similar behavior has also been reported in core/shell nanorod heterostructures that the higher growth temperature of the shell exhibit better thermal stability than that were synthesized at lower temperatures.^[33] In view of these advantages of high-temperature shell growth, CdSe-based core/shell NPLs not only act as a kind of highly stable light-emitting materials but also an excellent low-threshold gain medium for lasers. To date, the shell-thickness-dependent gain properties of CdSe/CdS core/shell NPLs synthesized by the high-temperature strategy have not been systematically studied. Understanding shell-thickness-dependent factors affecting gain performance in NPLs can provide guidelines to improve and even design better nanostructures as lasing media. Hence, the optical gain properties of such CdSe/CdS core/shell NPLs need to be further explored in depth for exploiting practical laser devices.

In this work, a series of shell-thickness-controlled CdSe/CdS core/shell NPLs have been synthesized by the hot-injection shell growth approach at a high temperature (300 °C). First of all, the effect of shell thickness on optical properties of CdSe/CdS NPLs is investigated. The NPLs with thicker CdS shells (6 MLs) exhibit the optimal ASE performance with an ultralow optical gain threshold as compared to the thinner ones.

However, as the shell thickness is further increased, ASE performance is worsened possibly for the reason of the increased number of strains induced defects. Moreover, the deeper insights into the excellent gain performance of thick-shell CdSe/CdS NPLs (6 MLs) are explored by using ultrafast transient absorption (TA) spectroscopy. Finally, thick-shell CdSe/CdS NPLs have been exploited as active medium to fabricate the vertical cavity surface-emitting laser (VCSEL) that realized a high beam quality single-mode lasing output with an ultralow threshold ($\approx 1.1 \mu\text{J cm}^{-2}$). Therefore, the results indicate that CdSe/CdS NPLs will be a promising lasing gain material for practical applications in semiconductor microlasers.

2. Results and Discussion

2.1. Structural and Optical Characterization of CdSe/CdS Core/Shell NPLs

In order to overcome limitations of conventional room-temperature approach for the optical properties of core/shell NPLs, CdSe/CdS core/shell NPLs were here prepared through high-temperature reactions (300 °C) with the low-reactivity Cd(oleate)₂ and 1-octanethiol as precursors. Briefly, we first synthesized four monolayers (≈ 1.2 nm) CdSe core NPLs with an emission at 513 nm, following a modified procedure reported previously.^[27] Figure 1a shows the schematic diagram of shell growth. By varying the precursor injection volume, we could precisely control over the thickness of CdS shells (see Section S1, Supporting Information). The photograph of NPLs under ultraviolet (UV) illumination exhibits the obvious emission changes with the reaction time. Figure 1b shows the absorption and emission spectra of CdSe core and CdSe/CdS core/shell NPLs with shell thickness of 3, 6, 9, and 14 MLs. These are all progressively shifted toward lower energy with the deposition of the CdS shell, because of the increasing delocalization of the electron into the shell region while the hole is mainly confined to the core.^[16,20] Moreover, the emission spectra of

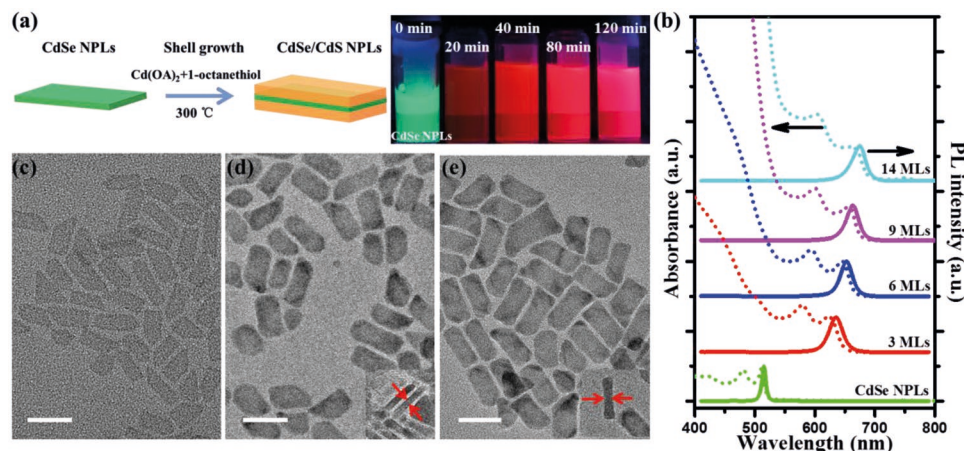


Figure 1. a) Schematic representation of the synthesis for CdSe/CdS core/shell NPLs, with photograph of core/shell NPLs samples at the different reaction time under UV illumination. b) Absorption and PL spectra of CdSe core and CdSe/CdS NPLs with different shell thickness. c–e) TEM images of CdSe core NPLs, 6 MLs, and 9 MLs CdSe/CdS NPLs. The inset shows the morphology of NPLs in vertical direction, the thickness is ≈ 4.9 and ≈ 6.8 nm for NPLs with 6 and 9 MLs, respectively. Scale bars are 30 nm.

CdSe/CdS NPLs could remain the narrower full-width at half maximum (FWHM) of ≈ 24 nm. The broadening of emission linewidth in these core/shell heterostructures is likely ascribed to the enhanced exciton–phonon coupling in the shell and the increased heterogeneity at the core/shell interface by atomic diffusion.^[16,34] The corresponding linewidths of single CdSe/CdS NPL (≈ 22 nm) shows a comparable value with the ensemble measurement (see Figure S1, Supporting Information), indicating the minimal heterogeneous broadening among NPLs. Importantly, the obvious absorption peaks are also observed both at the band edge and higher energies as the number of CdS MLs increases, suggesting that the thick-shell CdSe/CdS NPLs still kept more uniform thickness. Figure 1c–e and Figure S2 (Supporting Information) display the transmission electron microscopy (TEM) images of CdSe core and the corresponding CdSe/CdS core/shell NPLs, respectively. The morphologies of the initial CdSe NPLs are retained upon shell deposition. TEM images of vertically stacked NPLs could allow us experimentally to determine the NPLs thickness (inset in Figure 1d,e), implying that the CdS shells were indeed uniformly grown on both sides of the CdSe core NPLs. The vertical thickness of monodisperse CdSe/CdS NPLs could be measured up to ≈ 10 nm, which corresponds to that CdS shell thickness of ≈ 14 MLs (see Figure S2c, Supporting Information). Interestingly, we found that after the coating of CdS shells around the CdSe cores could further prevent the unwanted formation of extensive face-to-face stacks similar to core NPLs (see Figure S2a, Supporting Information), which would reduce the scattering losses and ultraefficient exciton-transfer-assisted exciton trapping in close-packed NPLs film.^[35,36]

The NPLs crystal structure is investigated in more detail with X-ray diffraction (XRD) measurements. Figure 2a shows the XRD patterns of these NPLs samples. The zinc-blende crystal structure of the CdSe NPLs was confirmed by three distinct diffraction peaks of CdSe cores are gradually shifted to CdS shell as the shell growth proceeds, and accompanied by a narrowing of diffraction peaks. The XRD spectrum indicates that the cubic zinc-blende phase of the initial CdSe core NPLs is reserved in thick-shell CdSe/CdS NPLs, which results in the formation of phase-pure CdSe/CdS NPLs and benefits to eliminate interfacial defects. Figure 2b shows PL decay traces of the CdSe core NPLs and their corresponding CdSe/CdS NPLs samples. The PL lifetime increases monotonically from 6 to 37 ns with the deposition of the CdS shell (see Figure S3, Supporting Information),

which was attributed to a reduction of electron–hole wavefunction overlap leading to a quasi-type-II band alignment of the CdSe/CdS structure.^[16,29,37] The dominated PL decay dynamics gradually tend to transfer from the multiexponential decay to single exponential decay with increasing shell thickness, demonstrating that the radiative decay component originating from the exciton trapping sites on the core surface are effectively passivated by the CdS shells.^[29,38]

PL quantum yields measurements (see Figure S3, Supporting Information) show that the QYs significantly increase with the CdS shell growth toward 6 MLs. The QYs of CdSe/CdS NPLs with 6 MLs was up to near $\approx 68\%$, suggesting that the surface trap states of NPLs are well-passivated by the highly crystalline CdS shell. However, with the formation of ultrathick CdS shells (>6 MLs), the QYs starts to gradually decrease. Besides further delocalization of electron wavefunction to the whole structure as a result of thicker shell growth, the decreased excitons recombination efficiency may also be related to the increasing probability of defect states at its surface/interface or inside the ultrathick CdS shells due to strain formation generated by the shell deposition,^[16,29,34] which was similar to the case in thick-shell CdSe/CdS quantum dots (QDs).^[39]

To investigate the effect of the CdS shell thickness on the in-solution photostability of CdSe/CdS NPLs, the NPLs hexane solutions were placed under a UV lamp (365 nm, 9 W). As shown in Figure 2c, the evolution of PL intensity of the CdSe-only and CdSe/CdS core/shell NPLs (3, 6, 9, and 14 MLs) was measured along with the UV illumination time. The PL intensities were normalized to the initial values of corresponding samples. The core-only NPLs emission reveals a large drop of $\approx 60\%$ after 12 h of UV illumination and gradually decreased to 10% of the initial intensity after exposure for 180 h. This phenomenon should be associated with the illumination-induced surface traps owing to the lack of protection of the core surface. The photostability of CdSe/CdS NPLs with 3 MLs shell is slightly improved. There is no longer the decreasing trend of emission intensity in comparison to core-only sample when the UV exposure time was sustained for 90 h. Obviously, the photostability of CdSe/CdS NPLs is dramatically enhanced upon further increasing shell thickness up to 6 MLs and 9 MLs, which ultimately keeps near 60% and 85% of the initial intensity, respectively. The NPL sample with 14 MLs CdS shells shows the best photostability, which can finally maintain over 95% of the original emission intensity after exposure for 180 h. These results demonstrate that relatively thick CdS shells could

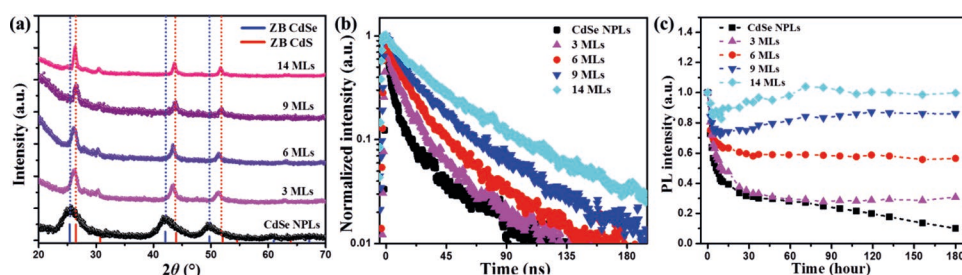


Figure 2. a) XRD patterns of the CdSe NPLs and CdSe/CdS NPLs with 3, 6, 9, and 14 MLs of CdS, the vertical solid lines indicate standard XRD patterns of zinc blende CdSe (blue) and CdS (red) bulk crystals. b) PL decay traces of CdSe NPLs and CdSe/CdS NPLs (3, 6, 9, and 14 MLs). c) Integrated PL intensities of CdSe cores and the corresponding CdSe/CdS NPLs as a function of UV exposure time.

largely improve the photostability of NPLs, indicating that thick CdS shell would more effectively protect the CdSe core emitters from the complicated surrounding environment or photodegradation during long-term light irradiation.

Besides the increased QYs and improved photostability based on CdS shell, the potentially enhanced optical absorption ability of CdS shells (in the short wavelength region <500 nm, see absorption spectra in Figure 1b) is expected to greatly increase the absorption cross section of core/shell NPLs, along with that CdS shell strongly transfers its exciton to the CdSe core. This type of rapidly efficient excitons transfer would contribute to lower optical gain threshold of exciton states in the CdSe core, as previously reported for colloidal core/crown NPLs and core/shell QDs.^[15,40] Meanwhile, the PL intensity measurement at a single NPL level (see Figure S4, Supporting Information) shows that PL blinking behavior could be better suppressed in thick-shell NPLs (6 MLs), the blinking behavior was commonly attributed to the nonradiative AR and the charge carrier trapping at surface and/or interface states.^[5,41] Therefore, thick-shell heterostructures from high-temperature shell growth exhibit efficient suppression of Auger process and trapping states with respect to the CdSe core-only NPLs. Additionally, the electron wavefunction in CdSe/CdS NPLs was allowed to spread over the whole core/shell structure for further reducing AR probability, thus helping to decrease nonradiative Auger losses of excitons and enhance the optical gain performance.^[25,30] So, the high-temperature strategy of thick CdS shells coating around

the CdSe core NPLs makes them to be greatly potential materials in NPL-based optoelectronic devices.

2.2. Amplified Spontaneous Emission Properties

All these advantages of CdSe/CdS core/shell NPLs could enable greatly benefit optical gain performance of NPLs. Here, the ASE properties of CdSe/CdS NPLs in close-packed films are studied to examine the shell-thickness-dependent optical gain properties (see Figure 3a,b and Figure S5, Supporting Information), under the stripe excitation at 400 nm (100 fs, 1 kHz). As the pump intensity increases, emission from the NPLs film edge exhibits a clear transition from spontaneous emission to ASE along with the feature of spectral narrowing (FWHM \approx 8–9 nm). At the same time, the ASE peaks for all samples are redshifted (5–17 nm) with respect to their spontaneous emission peak. This redshift in the observed ASE peak indicates the stimulated emission occurs from band edge biexciton states.^[12,13,29,42]

Figure 3c shows their corresponding emission intensity versus pump intensity monitored at the wavelength of ASE peaks. As the excitation intensities increase above the ASE thresholds, the output intensity shows a steep linear growth, a kind of characteristics of ASE. The shell-thickness-dependent ASE threshold value is shown in Figure 3d. In core-only CdSe NPLs, the average ASE threshold is \approx 22 $\mu\text{J cm}^{-2}$. The

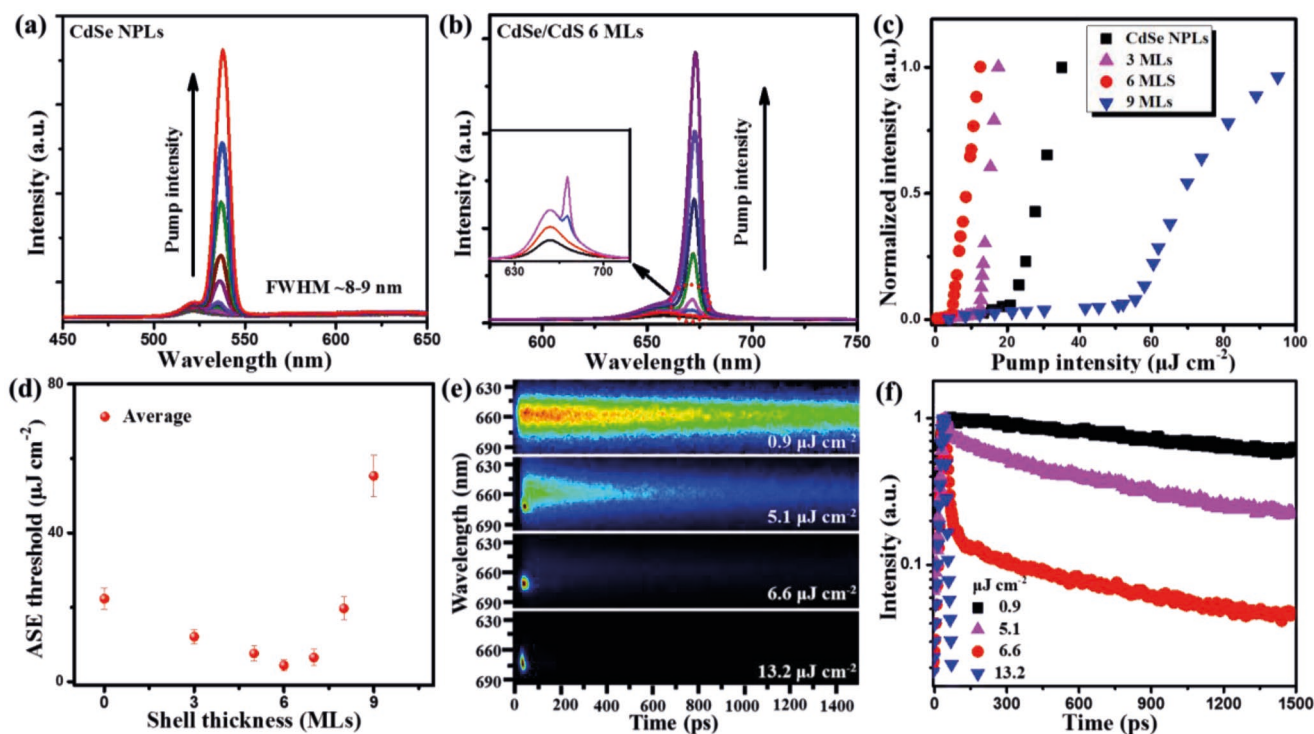


Figure 3. a,b) Emission spectra from a close-packed film of CdSe core NPLs and CdSe/CdS NPLs (6 MLs) with increasing pump intensities, the corresponding ASE peaks are detected at 537 and 671 nm, respectively. The inset shows the emission spectra of CdSe/CdS NPLs (6 MLs) near the ASE threshold. c) Emission intensity versus pump intensity at the positions of ASE and PL peaks for CdSe core and CdSe/CdS NPLs with 3, 6, and 9 MLs. d) Averaged ASE thresholds as a function of shell thickness. e) Time-resolved PL spectrogram of close-packed CdSe/CdS NPLs (6 MLs) film, measured with the pump intensity varying from lower than ASE threshold ($0.9 \mu\text{J cm}^{-2}$) to far above threshold ($13.2 \mu\text{J cm}^{-2}$). f) Transient emission decay traces extracted from spectrogram (e), measured at the position of emission peak.

ASE threshold for CdSe/CdS NPLs with 3 MLs CdS shell is decreased to $\approx 12 \mu\text{J cm}^{-2}$. With the further increase of shell thickness, the averaged stimulated emission threshold is derived to be as low as $\approx 4.4 \mu\text{J cm}^{-2}$ for the thick-shell CdSe/CdS NPLs with 6 MLs. This ASE threshold is one of the lowest values reported for II–VI core/crown ($4.15 \mu\text{J cm}^{-2}$)^[35] and core/shell (≈ 2.4 and $6 \mu\text{J cm}^{-2}$)^[20,43] NPL heterostructures, which is lower than the best previous reported values for phase-pure CdSe/CdS QDs ($16 \mu\text{J cm}^{-2}$) and CdSe-based core/alloy-layer/shell QDs ($\approx 6 \mu\text{J cm}^{-2}$)^[44,45] enables them to be highly promising candidates for low-threshold colloidal semiconductor lasing. However, an increased trend of ASE threshold is observed for CdSe/CdS NPLs with increasing CdS shells larger than 6 MLs. For ultrathick CdSe/CdS core/shell NPLs (14 MLs), the average ASE threshold is up to $\approx 176 \mu\text{J cm}^{-2}$.

The exceptionally low ASE threshold for thick-shell CdSe/CdS NPLs (6 MLs) compared to the core-only and thin-shell NPLs (3 MLs) can be explained by more effective surface passivation, suppressed AR, and enhanced absorption cross sections.^[13,20,22,30,31] The optical gain threshold increases in ultrathick-shell NPLs (>6 MLs) are likely attributed to the induced defects at the core/shell interface or inside the CdS shells by the release of strain with further increasing shells, which could quench the excitons transfer from the shell to the cores and weaken the suppression of AR.^[15,16,22,29,46] This would lead to an increased nonradiative loss of excitons before they relaxed into the core, and thus hindering the building up of population inversion in the CdSe core. Precisely because of these reasons, the threshold behavior of CdSe/CdS NPLs is almost consistent with the variation trend of shell-dependent QYs as mentioned before, which all exhibit the nonmonotonic dependence on the CdS shell thickness.

The transient PL dynamics of the ASE process in CdSe/CdS NPLs (6 MLs) was studied by a streak camera system (Figure 3e,f). Under the lower pump intensity ($0.9 \mu\text{J cm}^{-2}$), we only observe a long-lived PL decay trace of the spontaneous emission. When the pump intensity (5.1 and $6.6 \mu\text{J cm}^{-2}$) just increases above ASE threshold, a narrower ASE peak (≈ 8 – 9 nm) is appeared and gradually dominated by a much faster decay channel. As the pump intensity ($13.2 \mu\text{J cm}^{-2}$) far surpasses the threshold, the fast PL decay suddenly collapses to ≈ 11 ps, which is near the temporal resolution of streak camera system (see Figure S6, Supporting Information). Thus, the result reveals an ultrafast ASE process faster than 11 ps, which is enough to compete with the rapid Auger rates of the gain excited state.^[25]

2.3. Optical Gain Lifetime and Bandwidth

For more insights into the optical gain performance, the decay dynamics of the electronic states involved in the optical amplification process was usually investigated by the femtosecond TA measurement.^[13,20,47] Here, the ultrafast TA spectroscopy was employed to study the temporal dynamics of optical gain in CdSe/CdS NPLs (6 MLs) film. The TA spectra were measured by a variably delayed white light supercontinuum source with respective to the pump pulses.

Figure 4a–c shows the transient absorption spectrograms of thick-shell CdSe/CdS NPLs (6 MLs) under the pump intensity

of 3, 48, and $768 \mu\text{J cm}^{-2}$, respectively. At low pump intensity, we observe a long-lived bleached absorption band near the first and second excitonic absorption peak (Figure 4a). As the pump intensity increases, the photoinduced bleaching feature becomes gradually pronounced (Figure 4b,c). It is worth noting that the longest optical gain lifetime is observed close to the peak wavelength (671 nm) of ASE spectra (see Figure S7, Supporting Information), which is corresponding to the ASE region in NPLs, indicating that the optical gain here further comes into being stimulated emission. Accordingly, the TA spectra recorded at a delay time of 4 ps and the time evolution of TA spectra monitored at the ASE center wavelength are further extracted as a function of pump intensity, respectively. In TA spectra, optical gain can be achieved when the pump induced absorption bleach (ΔA) becomes greater than the linear absorption (A_0), shown as $\Delta A + A_0 < 0$. At the probe delay of 4 ps (Figure 4d), the optical gain amplitude decreases with the pump intensity and becomes < 0 after a pump intensity of $48 \mu\text{J cm}^{-2}$, indicating the presence of gain in the system. The gain amplitude starts to saturate after the pump intensity reaches $384 \mu\text{J cm}^{-2}$. At this point, the bandwidth of optical gain for CdSe/CdS NPLs exceeds 140 nm (inset in Figure 4d) owing to the participation of multiexciton states. For TA spectra monitored at the ASE peak of ≈ 671 nm (Figure 4e), the optical gain signals have nearly saturated when the pump intensity reaches $192 \mu\text{J cm}^{-2}$, which was primarily limited by the multiexciton AR and other nonradiative losses.^[13,20,48] Notably, the temporal analysis of the gain band shows that the lifetime of optical gain is sustained for more than 800 ps (inset in Figure 4e). Unlike in core-only NPLs, thick-shell NPLs could further extend the spatial separation of excitons in thickness dimensions, which lengthens the multiexciton state and gain lifetimes. As a result, the extremely long optical gain lifetime (>800 ps) of CdSe/CdS NPLs is ≈ 8 times larger than those previously reported core-only NPLs (≈ 100 ps)^[42,49] and also near two times greater than those of conventional CdSe/CdS QDs (>400 ps).^[50] Recently, such long optical gain lifetime (≈ 800 ps) is also reported in this novel CdSe/CdS@CdZnS core/crown@gradient-alloyed shell colloidal quantum wells.^[51] Therefore, thick-shell CdSe/CdS NPLs imply highly efficient optical gain performance, thus in favor of as an excellent gain material in NPL laser devices.

2.4. Single-Mode Lasing from the NPL-VCSEL

Here, the microlaser of the NPLs is developed based on a surface-emitting vertical resonant cavity device structure, which is a meaningfully preliminary exploration for their potential applications as low-threshold lasing materials in reality. We adopted a vertical cavity design consisting of a thick-shell CdSe/CdS NPLs (6 MLs) thin film and two high-reflectivity distributed Bragg reflector (DBR) mirrors. The cross-sectional scanning electron microscopy (SEM) image of the NPL-VCSEL device is shown in Figure 5a. The bottom DBR mirror was made out of 12 pairs of alternatively stacked SiO_2 and TiO_2 layers. High-quality NPL film ($\approx 1.36 \mu\text{m}$) was fabricated by drop-casting highly concentrated NPLs solutions onto one above-mentioned bottom DBR mirror. Then, a top DBR mirror (eight pairs alternating of CaF_2/ZnS layers) was deposited on

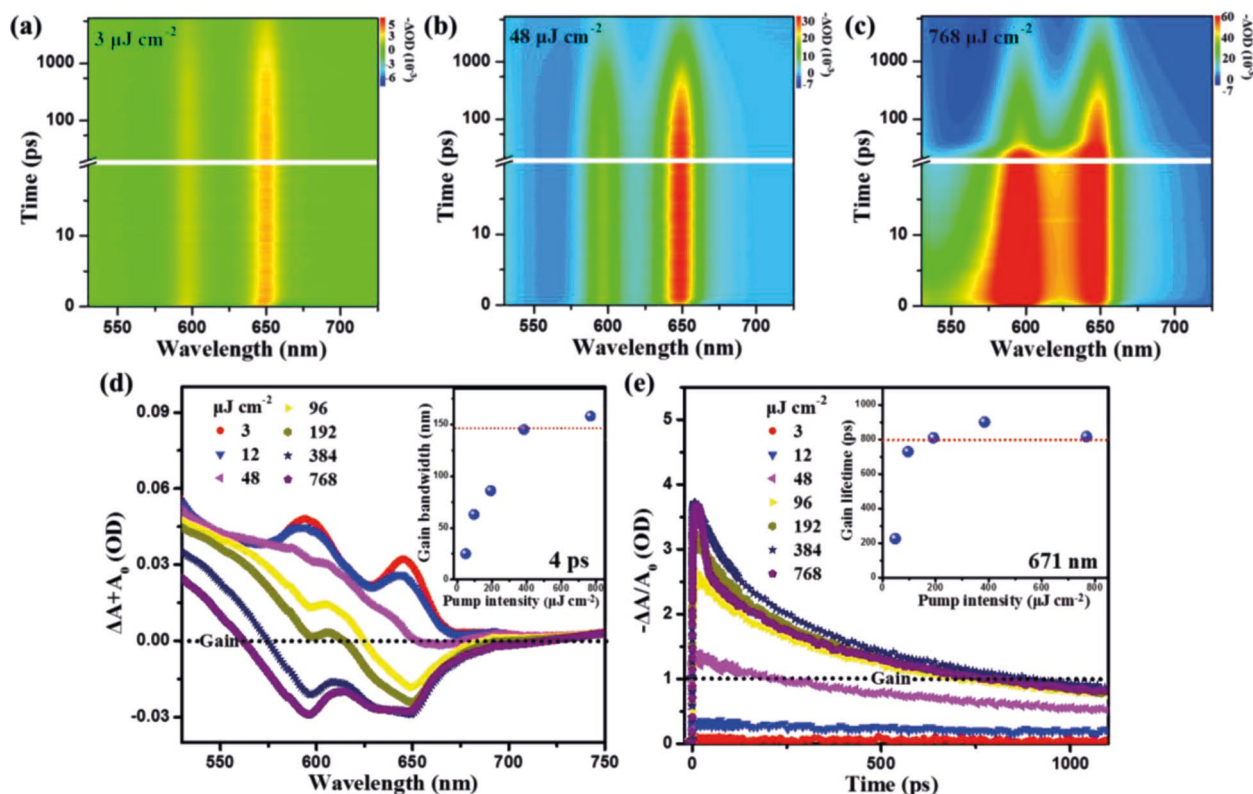


Figure 4. a–c) Transient absorption (TA) spectrograms for a CdSe/CdS NPLs (6 MLs) film under 400 nm excitation at 3, 48, and 768 $\mu\text{J cm}^{-2}$, respectively. The TA spectrum is manifested as a pronounced bleaching signal at high intensity pumping. d) Evolution of optical gain in pump dependence of nonlinear absorption changes ($\Delta A + A_0$) recorded at 4 ps delay time. The inset shows the bandwidth of optical gain versus pump intensity. e) Pump dependence of TA dynamics probed at 671 nm. The inset shows the lifetime of optical gain versus pump intensity.

top of NPL film by electron beam deposition (see the Experimental Section for the details of the device fabrication). Finally, we realize the whole microcavity with peak reflectivity over 99% (see Figure S8, Supporting Information), and the photograph of the final device is presented in Figure S9 (Supporting Information).

The schematic of the NPL-VCSEL in measurement is as shown in Figure 5b. The inset shows a photograph of the device in operation. The spatially directional emission from the VCSEL is observed with a bright and well-defined red spot perpendicular to device plane. Figure 5c shows the emission spectra of VCSEL with the progressively increased pump intensity. After the lasing threshold, sharp laser output is solely detected at ≈ 668 nm with a narrower FWHM of ≈ 2 nm that corresponds to a Q-factor of ≈ 334 . For a microcavity structure in this work, the large free spectral range (≈ 86 nm) is enough to ensure single-mode lasing operation inside the ASE band of the NPLs (see Section S12, Supporting Information). Besides the laser emission spectra and directional outputs, the features of lasing are also represented by the abrupt rising in output intensity after the pump intensity is above lasing threshold. The measurement result of emission intensity versus pump intensity is shown as the inset in Figure 5c, further confirming the lasing operation of the device. The ultralow lasing threshold is found to be as low as $\approx 1.1 \mu\text{J cm}^{-2}$, which is decreased to a quarter of the corresponding ASE threshold. Noteworthy, the momentum conservation is more

pronounced and AR rate was significantly diminished because of 1D confinement in NPLs.^[2,12] Hence, the lasing threshold for our NPL-VCSEL device ($\approx 1.1 \mu\text{J cm}^{-2}$) is lower than the best reported values for CdSe/CdS@CdZnS quantum wells ($\approx 7.5 \mu\text{J cm}^{-2}$) and phase-pure CdSe/CdS QDs ($\approx 2 \mu\text{J cm}^{-2}$) as well as CdSe/CdS quantum dot-in-rods ($\approx 10 \mu\text{J cm}^{-2}$) microlaser.^[44,51,52] In addition to the superior gain performance of thick-shell CdSe/CdS NPLs, the ultralow threshold lasing performance is also ascribed to the favorable coupling between the emission and the cavity modes inside such high-quality resonant cavity. To examine the emission stability of NPL-VCSEL, we continuously pumped the device up to 1.44×10^7 laser shots (1 kHz repetition rate), which corresponds to 4 h of continuous excitation (Figure S10, Supporting Information). The result shows that the laser emission intensity can retain above 90% of initial intensity after long duration of optical excitation (4 h), indicating excellent operation stability of the NPL-VCSEL device. For exploring a deeper insight into the lasing dynamics process in our device, we performed time-resolved PL spectrogram measurement on the CdSe/CdS NPLs VCSEL above the lasing threshold. The corresponding time-resolved PL intensity trace is shown in Figure 5d. The emission signal exhibits an ultrafast decay of ≈ 7 ps at central peak wavelength (668 nm), which is limited primarily by the response time of the streak camera system shown as the red curve, indicating that the lasing operation is mainly through a stimulated emission process.

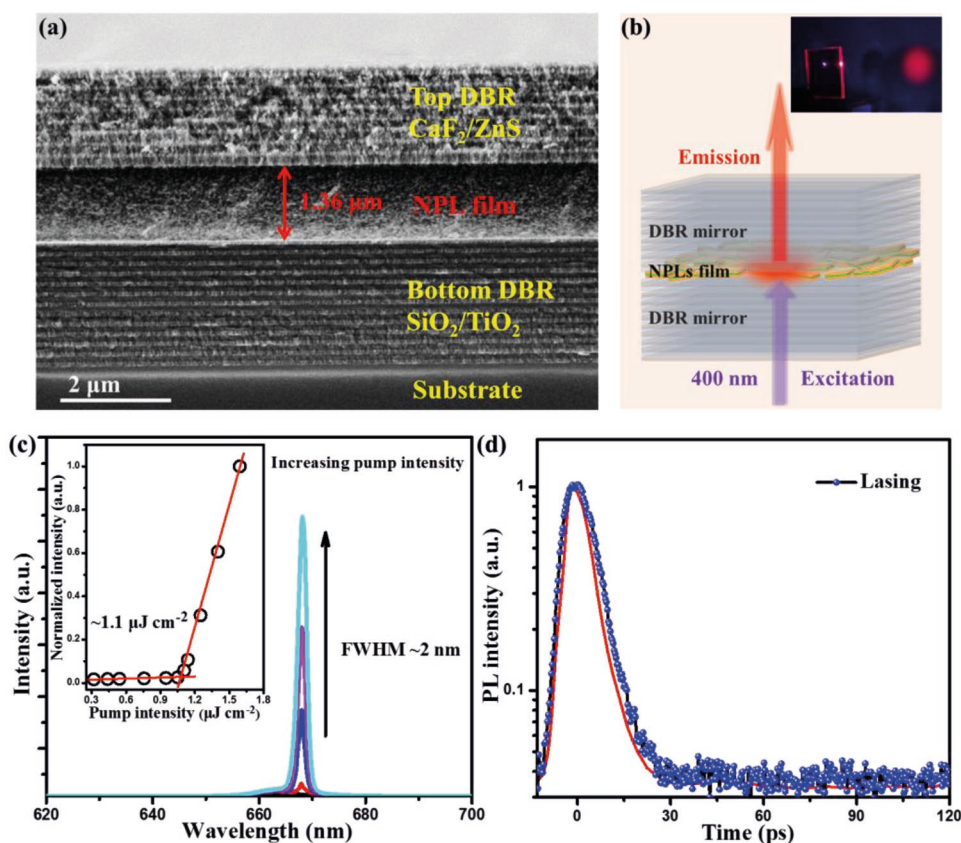


Figure 5. a) Cross-sectional SEM image of CdSe/CdS NPL-VCSEL device. b) Schematic of the VCSEL in measurement. Inset: Photograph of the VCSEL output beam in operation. c) Pump-intensity-dependent emission spectra from the device. Inset: Normalized emission intensity versus pump intensity, with the lasing threshold of $\approx 1.1 \mu\text{J cm}^{-2}$. d) PL time response above the lasing threshold. The red curve is the response time trace of the streak camera at the 160 ps range.

3. Conclusion

In conclusion, CdSe/CdS core/shell NPLs with different shell thickness have been synthesized by high-temperature shell growth approach. We have demonstrated that a protective CdS shells on the CdSe core NPLs effectively passivates surface trapping states and suppresses excitonic nonradiative recombination, thus increases the ensemble QYs and photostability. Meanwhile, the results indicate that thick-shell CdSe/CdS NPLs (6 MLs) exhibit the remarkable optical gain performance with an ultralow ASE threshold of $4.4 \mu\text{J cm}^{-2}$. Furthermore, the ultrafast TA measurements disclose the extraordinarily long gain lifetimes (>800 ps) and large gain bandwidth (>140 nm) in such core/shell NPLs. Finally, we have fabricated a VCSEL of thick-shell CdSe/CdS NPLs. The featuring single-mode output and directionality from the laser device are revealed clearly, together with an ultralow lasing threshold. Therefore, these results give us more insights into the shell-dependent optical gain performance in CdSe/CdS heterostructure NPLs and demonstrate that this core/shell NPL is a superior class of nanomaterials for optical gain and lasing. However, further optimizations are necessary in future works to eliminate the defects in the ultrathick-shell NPLs, such as engineering the core/gradient-alloyed layer/shell heterostructures to mitigate the excitons loss. This strategy is expected to further

improve gain performance and reduce lasing threshold, which may eventually realize the high-performance continuous-wave pumped or electrically driven colloidal NPL lasers.

4. Experimental Section

Synthesis of CdSe/CdS Core/Shell NPLs: CdSe/CdS core/shell NPLs were fabricated by optimizing the typical high-temperature synthesis approach,^[27,31] the shell thickness could be controlled through the amount of Cd- and S-precursors required for each ML. First, CdSe core NPLs (4 MLs) were synthesized using the reported recipe with slight modifications.^[27] Then, the CdS shells were epitaxially grown on the top and bottom surfaces of the CdSe core NPLs at high temperature (300°C).^[31] More information about the synthesis of CdSe/CdS core/shell NPLs, see the Supporting Information.

Fabrication of Core/Shell NPL-VCSEL Devices: Commercially available DBR mirrors were purchased as the bottom DBR, which consisted of 12 pairs of quarter-wavelength-thick $\text{SiO}_2/\text{TiO}_2$ layers deposited onto cleaned quartz substrates, with $\approx 99.5\%$ reflection for 671 nm. To obtain the high-quality CdSe/CdS NPLs (6 MLs) thin film, octane was added in the NPLs solution, and the volume ratio of octane to hexane was 1:5. To fabricate the VCSEL structure, highly concentrated NPLs solution dispersed in the mixed solvent of octane and hexane was drop-casted onto one bottom DBR mirror, which was ultrasonically cleaned by acetone and ethanol for 10 min, respectively. Then, the NPL layer was dried in the ambient environment and put into the vacuum axe keeping 24 h for further utilization. At last, a top DBR mirror (eight pairs of

alternating CaF₂/ZnS layers) with ≈99.2% reflection was deposited on top of NPL film by electron beam deposition at low temperature (40 °C). The thickness of each alternating CaF₂/ZnS layer was controlled to be a quarter of the wavelength at the emission peak.

Structural Characterizations: TEM image was obtained on a JOEL JEM-2100 electron microscope. The cross-sectional image of the VCSEL device was measured by Carl Zeiss Ultra Plus field emission SEM. XRD patterns were acquired using an X-ray diffractometer (Bruker, D8-DISCOVER) with Cu K α source.

Optical Measurements: PL spectra were recorded with a spectrofluorometer (RF-5301 PC, Shimadzu). The excitation wavelength was set to 400 nm. The absorption spectra were measured on a UV-vis-NIR spectrophotometer (UV3600, Shimadzu). The PL decay traces were recorded using an electrically triggered streak camera system (C5680, Hamamatsu). A femtosecond Ti:Sapphire laser with a frequency-doubling external β -barium borate crystal (400 nm, 1 kHz, 100 fs; Legend-F-1k, Coherent) was used as the pump sources. For the NPLs photostability measurements, the NPLs (in hexane solution) were placed under the UV illumination using a UV lamp (emission wavelength of 365 nm, power of 9 W). For the blinking measurements, a picosecond supercontinuum fiber laser (490 nm, 4.9 MHz; NKT Photonics EXR-15) was employed as the excitation source. The PL signal from a single NPL was collected by the confocal microscope and then sent to a single-photon counting system. The PL signal of a single NPL can be alternatively sent to a charge coupled device camera for the PL spectral measurements. For ASE measurements, a stripe pump (400 nm, 1 kHz, 100 fs) was acquired using a cylindrical lens (10 cm focal length). The stripe modal confined pump pulses were perpendicular to the surface of NPLs films, and then the emissions from the film edge were collected by the fast optical multichannel analyzer (OMA, SpectraPro-300i, Acton Research Corporation) and the optically triggered streak camera system (at the 1500 ps range) for steady and transient spectra, respectively. For the TA spectroscopy measurements, the femtosecond pump pulse was set to 400 nm. The excitons dynamics was probed through a broadband supercontinuum white-light source, which was generated via focusing a small portion of the femtosecond laser beam onto a sapphire plate. The TA signal was then recorded by a fast charge coupled device (S11071-1104, Hamamatsu) equipped with a monochromator (Acton 2358, Princeton Instrument). For the lasing and device stability measurements, the pump beam (400 nm, 1 kHz, 100 fs) was focused by a convex lens (5 cm focus length) onto the VCSEL, and the output signal was collected from the other side of the VCSEL along the normal direction by the OMA and optically triggered streak camera system (at the 160 ps range), respectively.

Supporting Information

Supporting Information is available from the Wiley Online Library or from the author.

Acknowledgements

This work was supported by the National Basic Research Program of China (973 Program, 2015CB352002), the Postgraduate Research & Practice Innovation Program of Jiangsu Province (KYCX17_0064), the Fundamental Research Funds for the Central Universities (2242017K41009, 2242018K41021), and the Science and Technology Support Program of Jiangsu Province (BE2018117, BE2016021).

Conflict of Interest

The authors declare no conflict of interest.

Keywords

amplified spontaneous emission, CdSe/CdS, nanoplatelets, optical gain, vertical cavity surface-emitting laser

Received: September 25, 2019

Revised: November 15, 2019

Published online:

- [1] S. Ithurria, B. Dubertret, *J. Am. Chem. Soc.* **2008**, *130*, 16504.
- [2] M. Pelton, *J. Phys. Chem. C* **2018**, *122*, 10659.
- [3] S. Ithurria, M. D. Tessier, B. Mahler, R. P. S. M. Lobo, B. Dubertret, Al. L. Efros, *Nat. Mater.* **2011**, *10*, 936.
- [4] S. Ithurria, G. Bousquet, B. Dubertret, *J. Am. Chem. Soc.* **2011**, *133*, 3070.
- [5] M. D. Tessier, C. Javaux, I. Maksimovic, V. Lorette, B. Dubertret, *ACS Nano* **2012**, *6*, 6751.
- [6] A. Naeem, F. Masia, S. Christodoulou, I. Moreels, P. Borri, W. Langbein, *Phys. Rev. B: Condens. Matter Mater. Phys.* **2015**, *91*, 121302.
- [7] J. Feldmann, G. Peter, E. O. Göbel, P. Dawson, K. Moore, C. Foxon, R. J. Elliott, *Phys. Rev. Lett.* **1987**, *59*, 2337.
- [8] A. Yeltik, S. Delikanli, M. Olutas, Y. Kelestemur, B. Guzelurk, H. V. Demir, *J. Phys. Chem. C* **2015**, *119*, 26768.
- [9] Z. Chen, B. Nadal, B. Mahler, H. Aubin, B. Dubertret, *Adv. Funct. Mater.* **2014**, *24*, 295.
- [10] F. Fan, P. Kanjanaboos, M. Saravanapavanantham, E. Beauregard, G. Ingram, E. Yassitepe, M. M. Adachi, O. Voznyy, A. K. Johnston, G. Walters, G.-H. Kim, Z.-H. Lu, E. H. Sargent, *Nano Lett.* **2015**, *15*, 4611.
- [11] U. Giovannella, M. Pasini, M. Lorenzon, F. Galeotti, C. Lucchi, F. Meinardi, S. Luzzati, B. Dubertret, S. Brovelli, *Nano Lett.* **2018**, *18*, 3441.
- [12] J. Q. Grim, S. Christodoulou, F. Di Stasio, R. Krahne, R. Cingolani, L. Manna, I. Moreels, *Nat. Nanotechnol.* **2014**, *9*, 891.
- [13] C. She, I. Fedin, D. S. Dolzhanikov, P. D. Dahlberg, G. S. Engel, R. D. Schaller, D. V. Talapin, *ACS Nano* **2015**, *9*, 9475.
- [14] B. T. Diroll, D. V. Talapin, R. D. Schaller, *ACS Photonics* **2017**, *4*, 576.
- [15] B. Guzelurk, Y. Kelestemur, M. Olutas, S. Delikanli, H. V. Demir, *ACS Nano* **2014**, *8*, 6599.
- [16] M. D. Tessier, B. Mahler, B. Nadal, H. Heuclin, S. Pedetti, B. Dubertret, *Nano Lett.* **2013**, *13*, 3321.
- [17] F. T. Rabouw, J. C. van der Bok, P. Spinicelli, B. Mahler, M. Nasilowski, S. Pedetti, B. Dubertret, D. Vanmaekelbergh, *Nano Lett.* **2016**, *16*, 2047.
- [18] K. Wu, Q. Li, Y. Jia, J. R. McBride, Z.-X. Xie, T. Lian, *ACS Nano* **2015**, *9*, 961.
- [19] B. Guzelurk, Y. Kelestemur, M. Olutas, Q. Li, T. Lian, H. V. Demir, *J. Phys. Chem. Lett.* **2017**, *8*, 5317.
- [20] C. She, I. Fedin, D. S. Dolzhanikov, A. Demortière, R. D. Schaller, M. Pelton, D. V. Talapin, *Nano Lett.* **2014**, *14*, 2772.
- [21] C. E. Rowland, I. Fedin, B. T. Diroll, Y. Liu, D. V. Talapin, R. D. Schaller, *J. Phys. Chem. Lett.* **2018**, *9*, 286.
- [22] M. Pelton, J. Andrews, I. Fedin, D. V. Talapin, H. Leng, S. K. O'Leary, *Nano Lett.* **2017**, *17*, 6900.
- [23] X. D. Ma, B. T. Diroll, W. J. Cho, I. Fedin, R. D. Schaller, D. V. Talapin, S. K. Gray, G. P. Wiederrecht, D. J. Gosztola, *ACS Nano* **2017**, *11*, 9119.
- [24] B. Mahler, B. Nadal, C. Bouet, G. Patriarche, B. Dubertret, *J. Am. Chem. Soc.* **2012**, *134*, 18591.
- [25] L. T. Kunneman, M. D. Tessier, H. Heuclin, B. Dubertret, Y. V. Aulin, F. C. Grozema, J. M. Schins, L. D. A. Siebbeles, *J. Phys. Chem. Lett.* **2013**, *4*, 3574.

- [26] S. Ithurria, D. V. Talapin, *J. Am. Chem. Soc.* **2012**, *134*, 18585.
- [27] C. Meerbach, R. Tietze, S. Voigt, V. Sayevich, V. M. Dzhagan, S. C. Erwin, Z. Dang, O. Selyshchev, K. Schneider, D. R. T. Zahn, V. Lesnyak, A. Eychmüller, *Adv. Opt. Mater.* **2019**, *7*, 1801478.
- [28] S. Yadav, A. Singh, L. Thulasidharan, S. Sapra, *J. Phys. Chem. C* **2018**, *122*, 820.
- [29] Y. Kelestemur, B. Guzelturk, O. Erdem, M. Olutas, K. Gungor, H. V. Demir, *Adv. Funct. Mater.* **2016**, *26*, 3570.
- [30] Y. Altintas, U. Quliyeva, K. Gungor, O. Erdem, Y. Kelestemur, E. Mutlugun, M. V. Kovalenko, H. V. Demir, *Small* **2019**, *15*, 1804854.
- [31] A. A. Rossinelli, A. Riedinger, P. Marques-Gallego, P. N. Knüel, F. V. Antolinez, D. J. Norris, *Chem. Commun.* **2017**, *53*, 9938.
- [32] O. Chen, J. Zhao, V. P. Chauhan, J. Cui, C. Wong, D. K. Harris, H. Wei, H. Han, D. Fukumura, R. K. Jain, M. G. Bawendi, *Nat. Mater.* **2013**, *12*, 445.
- [33] B. T. Diroll, C. B. Murray, *ACS Nano* **2014**, *8*, 6466.
- [34] J. Cui, A. P. Beyler, I. Coropceanu, L. Cleary, T. R. Avila, Y. Chen, J. M. Cordero, S. L. Heathcote, D. K. Harris, O. Chen, *Nano Lett.* **2016**, *16*, 289.
- [35] D. Dede, N. Taghipour, U. Quliyeva, M. Sak, Y. Kelestemur, K. Gungor, H. V. Demir, *Chem. Mater.* **2019**, *31*, 1818.
- [36] B. Guzelturk, O. Erdem, M. Olutas, Y. Kelestemur, H. V. Demir, *ACS Nano* **2014**, *8*, 12524.
- [37] F. Rajadell, J. I. Climente, J. Planelles, *Phys. Rev. B* **2017**, *96*, 035307.
- [38] L. T. Kunneman, J. M. Schins, S. Pedetti, H. Heuclin, F. C. Grozema, A. J. Houtepen, B. Dubertret, L. D. A. Siebbeles, *Nano Lett.* **2014**, *14*, 7039.
- [39] L. Zhang, H. Li, C. Liao, H. Yang, R. Xu, X. Jiang, M. Xiao, C. Lu, Y. Cui, J. Zhang, *J. Phys. Chem. C* **2018**, *122*, 25059.
- [40] F. García-Santamaría, Y. Chen, J. Vela, R. D. Schaller, J. A. Hollingsworth, V. I. Klimov, *Nano Lett.* **2009**, *9*, 3482.
- [41] Al. L. Efros, D. J. Nesbitt, *Nat. Nanotechnol.* **2016**, *11*, 661.
- [42] Q. Li, T. Lian, *Chem. Sci.* **2018**, *9*, 728.
- [43] Y. Altintas, K. Gungor, Y. Gao, M. Sak, U. Quliyeva, G. Bappi, E. Mutlugun, E. H. Sargent, H. V. Demir, *ACS Nano* **2019**, *13*, 10662.
- [44] C. Liao, R. Xu, Y. Xu, C. Zhang, M. Xiao, L. Zhang, C. Lu, Y. Cui, J. Zhang, *J. Phys. Chem. Lett.* **2016**, *7*, 4968.
- [45] Y. S. Park, W. K. Bae, T. Baker, J. Lim, V. I. Klimov, *Nano Lett.* **2015**, *15*, 7319.
- [46] Q. Li, K. Wu, J. Chen, Z. Chen, J. R. McBride, T. Lian, *ACS Nano* **2016**, *10*, 3843.
- [47] V. I. Klimov, A. A. Mikhailovsky, S. Xu, A. Malko, J. A. Hollingsworth, C. A. Leatherdale, H. J. Eisler, M. G. Bawendi, *Science* **2000**, *290*, 314.
- [48] Y. Xu, Q. Chen, C. Zhang, R. Wang, H. Wu, X. Zhang, G. Xing, W. W. Yu, X. Wang, Y. Zhang, M. Xiao, *J. Am. Chem. Soc.* **2016**, *138*, 3761.
- [49] Q. Li, Q. Liu, R. D. Schaller, T. Lian, *J. Phys. Chem. Lett.* **2019**, *10*, 1624.
- [50] M. Marceddu, M. Saba, F. Quochi, A. Lai, J. Huang, D. V. Talapin, A. Mura, G. Bongiovanni, *Nanotechnology* **2012**, *23*, 015201.
- [51] N. Taghipour, S. Delikanli, S. Shendre, M. Sak, M. Li, F. Isik, I. Tanriover, B. Guzelturk, T. C. Sum, H. V. Demir, *arXiv preprint* **2019**, arXiv:1906.06913.
- [52] F. Di Stasio, J. Q. Grim, V. Lesnyak, P. Rastogi, L. Manna, I. Moreels, R. Krahn, *Small* **2015**, *11*, 1328.